IJL, Vol. 25, Issue 1, 2026
http://doi.org/10.31900/ijl.v25i1.556

Research Article

IRAQI JOURNAL OF LASER

The Plasmonic Influence on the Performance of Laser-Scribed Front-Contact Gold Layer in Ultra-Thin Film Silicon Solar Cell

Rusul A. Dahab* and Hussein A. Jawad

Institute of Laser for Postgraduate Studies/ University of Baghdad/Baghdad/Iraq.
**Email address of the Corresponding Author: rusul.ahmed2301m@ilps.uobaghdad.edu.iq*

Article history: Received 23 Dec. 2025, Accepted 1 Mar. 2026, Published online 15 Jun. 2026

Abstract: Laser scribing of the front-layer metal contact in thin-film silicon solar cell is one method that enhances optical absorption through localized surface plasmon resonance (LSPR) induced at the laser-scribed gold nano-grooves. A new approach investigates both the plasmonic effect and increasing the absorption of the gold via laser scribing to improve the cell performance. A 3D ultra- thin film silicon solar cell (dimensions of $400 \times 400 \times 900$ nm^3 for width, length, and height) was designed, with a 50 nm thick gold front contact scribed at groove depths of 10, 20, 30, and 40 nm (fixed width of 100 nm). COMSOL Multiphysics software version 6.2, using the finite element method (FEM), was employed to design and numerically investigate the proposed cell. The results revealed a maximum photocurrent of 24.66 mA/cm^2 at a scribed depth of 40 nm. The laser-scribed nano-grooves excite localized surface plasmon resonances at the gold-silicon interface, enhancing electromagnetic field confinement and light trapping in the ultra-thin silicon layer. It is concluded that the laser scribing of the front gold contact improves the light absorption, leading to a significant increase in photo-generation rate and photocurrent density due to plasmonic field enhancement.

Keywords: COMSOL Multiphysics, Laser scribing, Plasmonic, Silicon.

1. Introduction

Recent global economic development has led to adverse climate changes. Therefore, efficient renewable energy sources are in high demand [1,2]. Currently, solar cells represent the essential devices that depend on the photovoltaic materials, ranging from p-n junction solar cells to dye solar cells (DSCs). DSCs have gained wide interest due to several reasons, including their environmental friendliness, low energy fabrication, and low cost, but their efficiency remains limited (maximum reported of 13 %). Perovskite solar cells improved efficiency to, 22.1 % but stability over long period is poor compared to conventional cells, which ordinary work for 25 years [3, 4].

The substantial components of the optical electronics are the semiconductor devices, including various applications such as photodetectors, photodiodes, photo sensors, and solar cells. Those devices are essential for optoelectronic, where they are distinguished by tunable properties that have attracted a great interest of researchers [5, 6]. Silicon solar cells emerged among the mentioned sources because of the low cost of the engineering process and their affinity with adaptable substrates [7].

The main issue with first-generation silicon solar cells is the active layer thickness (100 to 300 micrometers), requiring high-purity silicon and increasing costs [8]. Researchers developed thin-film solar cells to reduce thickness as much as possible, but this decreased absorption length and efficiency. Current efforts focus on maximizing absorption thin-film solar cells. A new problem

appeared, represented by the reduction of the absorption thickness of the active layer. As a result, the length of effective absorption is reduced, and for sure, the efficiency of the cell is decreased. The next purpose of the researchers is to find a certain method to increase the optical path length. The recent research works are focused on the design of thin-film solar cells with maximum absorption, without ignoring their efficiency [9-11]. The plasmonic effect enhances solar cell performance by increasing the field intensity, and hence, the produced photocurrent. In p-n junction silicon solar cells, plasmons raise light absorption, reduce exciton energy (improving photocurrent), and lengthened absorption paths (leading to increase current and voltage). Plasmonics significantly enhances efficiency [12].
The front contact of ultra-thin film solar cells affects light absorption and the efficiency, therefore, various structures were designed for this purpose. Laser-scribed metal contacts are promising, as this non-contact method minimizes damage and contamination. Laser scribing increases exposed surface area, raising absorption. The efficiency of the solar cells could be increased by laser scribing through the reduction in the optical losses. To ensure long-term stability of the scribed module, different factors should be taken into account, including the criteria of grooves and the balance between the optical and electrical losses [13, 14]. The scribing of the front layer is increasing the surface area that is exposed to the incident light, leading to raise the rate of absorption. The gold nanoparticles are widely used in solar cell due to its unique optical and electrical properties. Gold nanoparticles enhance absorption via plasmonic effect. Because of the small front-layer contact area of the thin-film solar cell, the surface area should be enlarged to get higher efficiency. The previous studies used laser scribing for the variation of the structures which cannot be obtained through traditional methods. The present work investigates the possibilities of laser scribing to get a larger surface area within similar dimensions. A new approach is investing both the plasmonic effect and increasing the absorption of the gold via laser scribing to enhance the cell performance. This work is to design and investigate an ultra-thin film silicon solar cell with a laser-scribed gold front contact to increase the optical absorption.

2. The proposed cell

The structure of ultra-thin film silicon with Laser- scribed gold layer solar cell was designed. COMSOL Multiphysics software version 6.2, using the finite element method (FEM), Electromagnetic field, Frequency Domain (EWFD), was performed to study the optical properties of the suggested design numerically, as shown in Fig. 1.

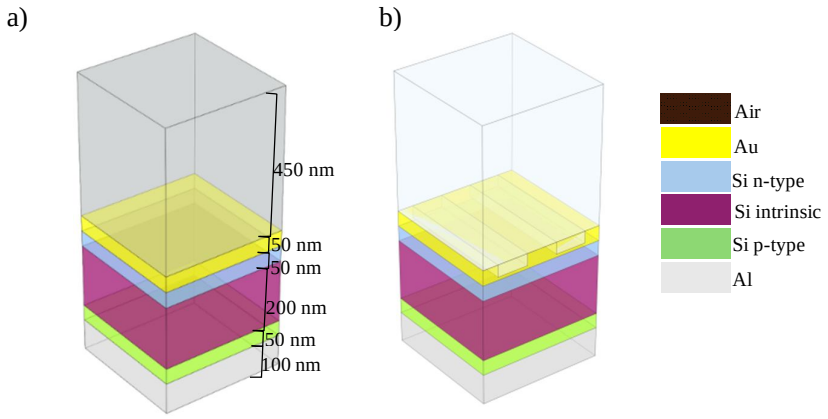

Fig. 1: The design of silicon solar cell, a) with a gold layer front contact, b) with a scribed gold front contact.

The structure of the proposed cell consisted of Au (front contact, n, k from Werner et al, 2009, 0.0176-2.48 µm), n-type Si Silicon ETL [600 Ω-cm], p-type Si, active layer/HTL (n, k from Shkondin et al.,

2017, 2-20 µm), (14 ohm-cm) and Al back reflector contact (McPeak et al., 2015). The energy band of the silicon solar cell is depicted in Fig. 2.

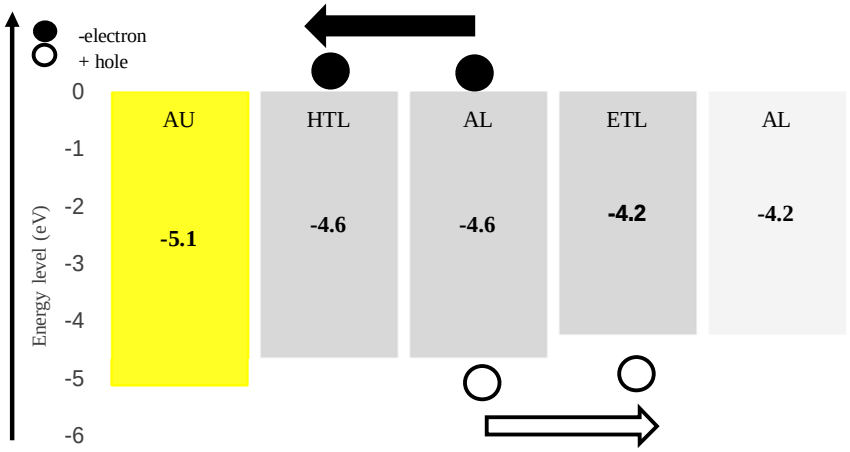

Fig. 2: Energy bands of the proposed cell.

Layer thicknesses were 450 nm air, 50 nm Au, 50 nm ETL, 200 nm AL, 50 nm HTL, and 100 nm Al from top to bottom. Cell dimensions of the cell were 400 × 400 × 900 nm³. A plane wave (y-polarized, normal incidence along z) illuminated the cell under AM1.5G spectrum (300-1300 nm, 10 nm steps). Periodic boundary conditions (PBCs, 900 nm period, Floquet type) applied in x-y direction, perfect electric conductor (PEC) on Al back. They acted as a back reflector to reflect the incident light to be absorbed again. The utilized mesh was set on a User-controlled, finer elements (max 49.5 nm, min 3,6), swept for Al/HTL/air, tetrahedral for active/ETL/Au. The width between the grooves was fixed at 100 nm, related to the gold layer width and the focal spot diameter of the laser used. To observe the effect of the groove dimension on the absorption of the cell, different depths were chosen (10-40) nm, as shown in Fig. 3.

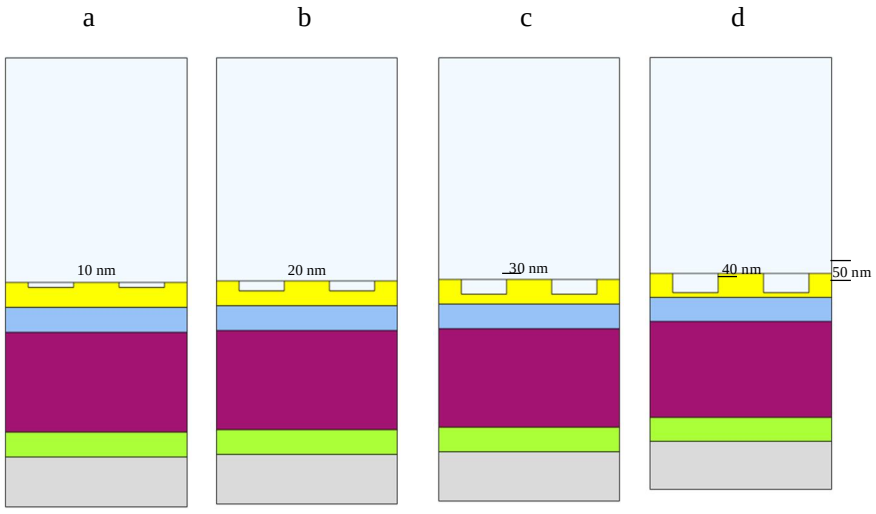

Fig. 3: The proposed cell with scribing laser groove on the front contact at varying depths: (a) 10 nm, (b) 20 nm, (c) 30 nm, and (d) 40 nm.

The optical properties of different structures used in the current study were investigated and analyzed, including (optical absorption, photo-generation rate, photocurrent density, and electric field distribution profile).
The light absorption and electromagnetic field (EM) distribution were calculated and simulated by solving the well-established Helmholtz equation $\nabla \times \nabla \times \vec{E} - k_0^2 \epsilon_r \vec{E} = 0$ [15], where K_0 is the wave vector of the incident light, ϵ_r is the dielectric permittivity of the concerned medium.
Reflection *(R(ω))* and transmission *(T(ω))* monitors were installed above and below the structure to measure the absorption *(A(ω))* by Eq. (1) [16]:

$$A(\omega) = 1 - R(\omega) - T(\omega) \quad (1)$$

The calculation of the power absorbed density in a unit cell is illustrated in Eq. (2):

$$P_{abs}(\lambda) = 0.5\omega |E(\omega)|^2 Im(\epsilon(\omega)) \quad (2)$$

The optical carrier generation rate is the number of photons absorbed in the ultra-thin film silicon solar cell per unit volume G_{ph}, and was calculated by Eq. (3) [16]:

$$G_{ph} = \int_{300}^{1300} \frac{P_{abs}}{hc/\lambda} d\lambda \quad (3)$$

Where $|E(\omega)|$ and *Im((ω))* is the electric field at angular frequency ω and the imaginary part of the dielectric constant of the material, respectively [17]. The photocurrent could be calculated as Eq. (4) [12]:

$$J_{ph}(\lambda) = \frac{e\lambda}{hc} \int_{300}^{1300} P_{abs} I_{AM.1.5}(\lambda) d\lambda \quad (4)$$

3. Result and discussion

The simulation results for the proposed cell with a 50 nm thick gold layer thickness and the solar cell with a scribed gold layer are presented and analyzed. The investigation covered normalized absorption, photo-generation rate, photocurrent density, and electric field distribution.

3.1. Normalized absorption

The normalized absorption was calculated using Eq. (2). Fig. 4 shows the absorption spectra for the proposed cell and the reference with a scribed layer. Normalized absorption as a function of wavelength is shown for different groove depths (10, 20, 30, and 40 nm).
Resonance wavelengths appeared at 400, 490, and 650 nm in the visible region, plus one peak in the IR region at 1050 nm. These optical absorptions clearly indicated the effect of plasmonic LSPR. Absorption of the resonance wavelength increased with groove depth. An IR shift in the resonance wavelength was observed with increasing depth.
This is attributed to plasmonic effect in the gold layer, which became prominent as light penetrates deeply. LSPR also indicated indication of the near-field intensity. The depth of 40 nm gives the highest absorption. The resonance wavelengths are a little bit shifted to IR. The normalized absorption for all resonance wavelengths at different depths is illustrated in Table 1.
Maximum absorption values corresponding to the groove depth are 0.39, 0.5, 0.81, and 0.87 for 10, 20, 30, and 40 nm, respectively. The influence of the groove depth on the optical absorption is shown in Fig. 5. A linear increase was observed, with maximum absorption at 40 nm. This is expected because increasing groove depth reduces the effective gold thickness, directly enhancing light absorption and revealing the plasmonic effect. Subtracting the 40 nm groove depth from the 50 nm gold thickness leave 10 nm, which supports the LSPR and enhances the plasmonic effect. Maximum normalized absorption values as a function resonance wavelength and depth are shown in Fig. 6.

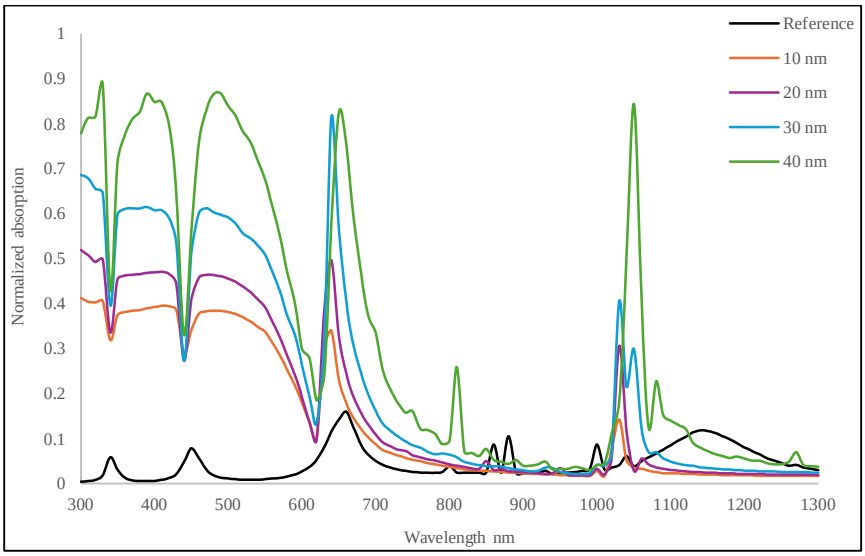

Fig. 4: Normalized absorption for the scribed laser with different groove depth (10, 20, 30, and 40) nm with the reference cell.

Table 1. Normalized absorption at each groove depth and resonance wavelengths.

λ (nm)	A (10 nm)	A (20 nm)	A (30 nm)	A (40 nm)
400	0.39	0.47	0.62	0.87
490	0.38	0.46	0.6	0.87
650	0.23	0.5	0.81	0.82
1050	0.14	0.31	0.4	0.84

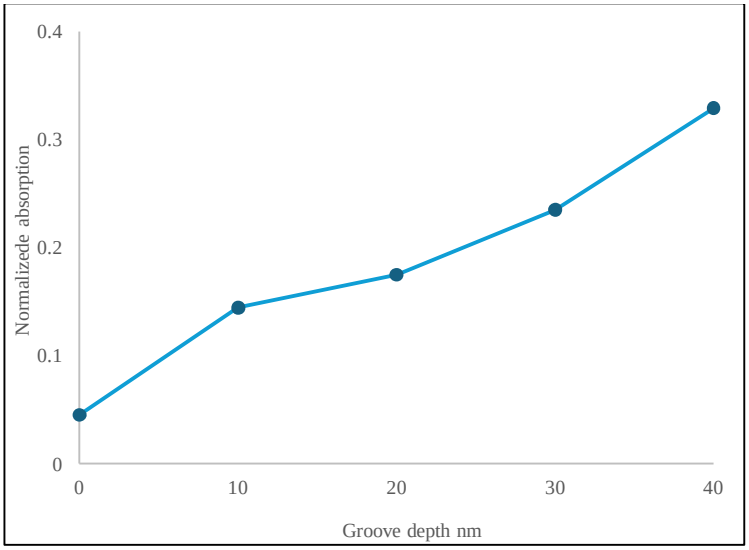

Fig. 5: Normalized absorption for the scribed laser with different groove depth (10, 20, 30, and 40) nm with the reference cell.

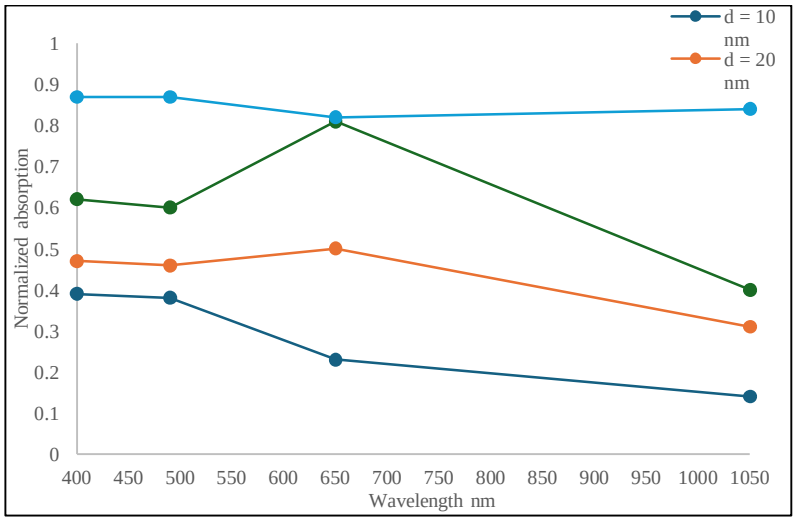

Fig. 6: Maximum normalized absorption for all resonance wavelengths at various depths (10, 20, 30, and 40) nm.

3.2. Photo-generation rate

Photo-generation rate as a function of wavelength is shown in Fig. 7, (based on Eq. 6). Similar behavior was observed across cases, with the maximum at 1050 nm, with decreasing toward shorter wavelengths and a minimum at 420 nm. Groove depth clearly influences the photo-generation rate, with deeper grooves yielding higher as absorption increases toward the electron transport layer. Surface plasmon polariton became prominent. Incident light on the gold surface, raises absorption via local surface plasmon polariton (near-field) or by scattering (far-field).

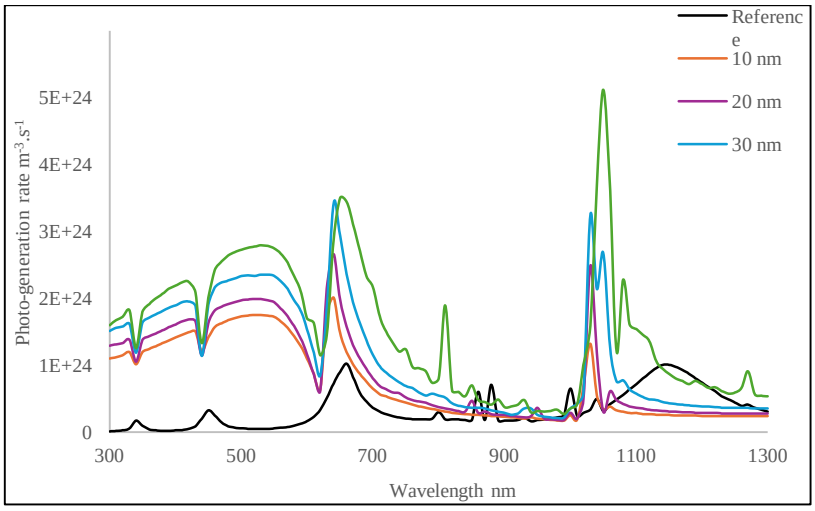

Fig. 7: Spectra of photo-generation rate for the scribed laser with different groove depth (10, 20, 30, and 40) nm with the reference cell.

The impact of groove depth on photo-generation rate is shown in Fig. 8. Similar behavior of normalized absorption was observed, remaining linear regardless of absolute values at each wavelength.

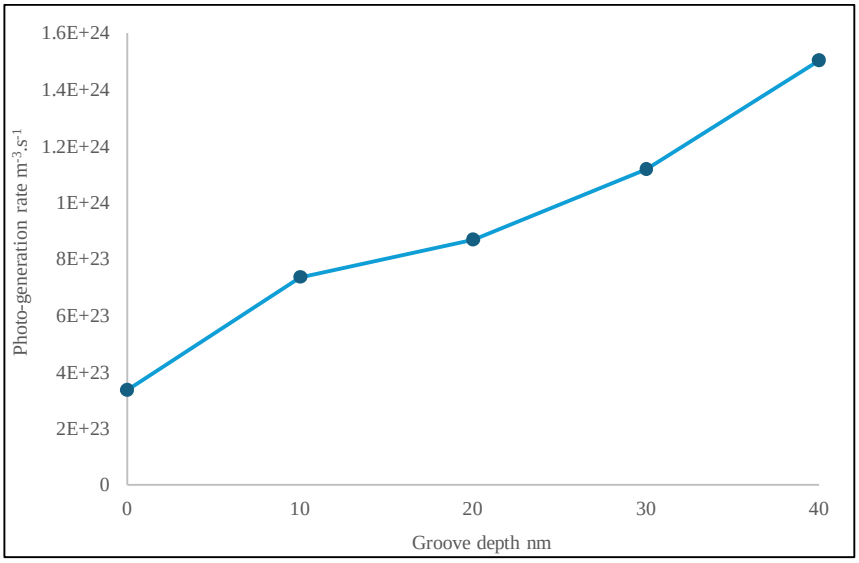

Fig. 8: Photo-generation rate for the scribed laser with different groove depth (10, 20, 30, and 40) nm with the reference cell.

Photo-generation rate represents the number of electron-hole pairs per unit volume per unit time due to the absorption of the light. Plasmonic enhanced absorption, therefore, increased the photogeneration rate.

3.3 Photocurrent density

Cell efficiency of the proposed ultra-thin film silicon solar cell with a scribed gold layer is determined by the produced photocurrent using Eq. (4) Fig. 9 shows the photocurrent versus the related wavelength. Here, the maximum photocurrent is detected at 660 nm, decreasing toward shorter wavelength then decreased toward shorter wavelengths, with another peak at1050 nm in the IR region. Photocurrent enhancement was due to increase absorption in the flowing mechanism: higher photo-generated rate, and thus greater photocurrent. This behavior is mainly influenced by the distribution of the incident light on the solar cell (A.M 1.5 G), with two peaks at 650 and 1050 nm matching high intensity region.

This wavelength was located in the maximum spectral intensity region of the incident light. It was noticed that the photocurrent of the proposed cell increased in comparison to the reference cell with a plane gold layer, indicating clearly the effect of the absorption of the incident light through the large surface area, regardless of the groove depth. Deeper grooves yielded higher photocurrent at all resonance wavelengths. Visible spectral region contributions improved overall performance related to IR. Groove depth impact on the photocurrent density was also investigated. The photocurrent density versus groove depth is shown in Fig. 10, with linear behavior.

According to equations (1), (3), and (4), photocurrent depends on the photo-generation rate, which is tied to the light absorption of the incident light.

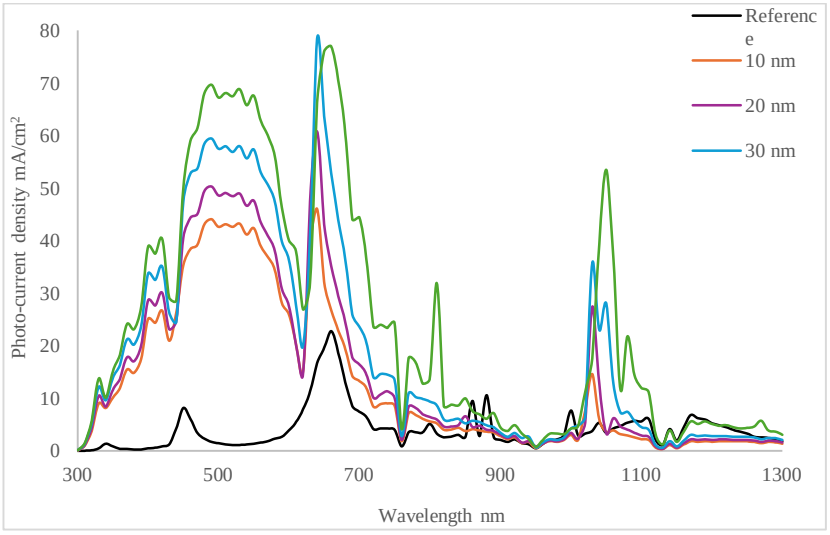

Fig. 9: Spectra of photocurrent density for the scribed laser with different groove depth (10, 20, 30, and 40) nm with the reference cell.

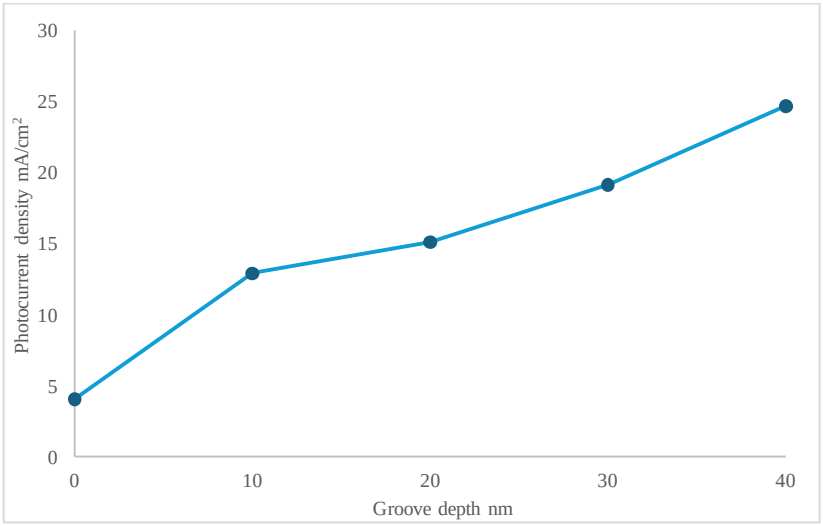

Fig. 10: Photocurrent density for the scribed laser with different groove depth (10, 20, 30, and 40) nm with the reference cell.

3.4 . Electric field distribution

Electric field scattering is related to absorption region, with maximum value at plasmonic sites (near-field LSPR or far-field scattering). Combining o LSPR (near-field enhancement) and far-field scattering (redirected light for absorption) enhance the performance of the cell. Distribution at resonance wavelengths are shown in Figs 11-14 for visible (400, 490, and 620 nm) and IR (1050 nm).

It was observed that the electric field distribution concentrated on the gold, was the strongest at groove depth edges. The difference in the field distribution intensity is related to their absorption, and the highest intensity field was observed in the deepest grooves (40 nm). Table 2 demonstrates the results of normalized absorption (A), photo-generation rate (G_{ph}), and photocurrent density (J_{ph}) for the proposed cell in comparison to the reference cell.

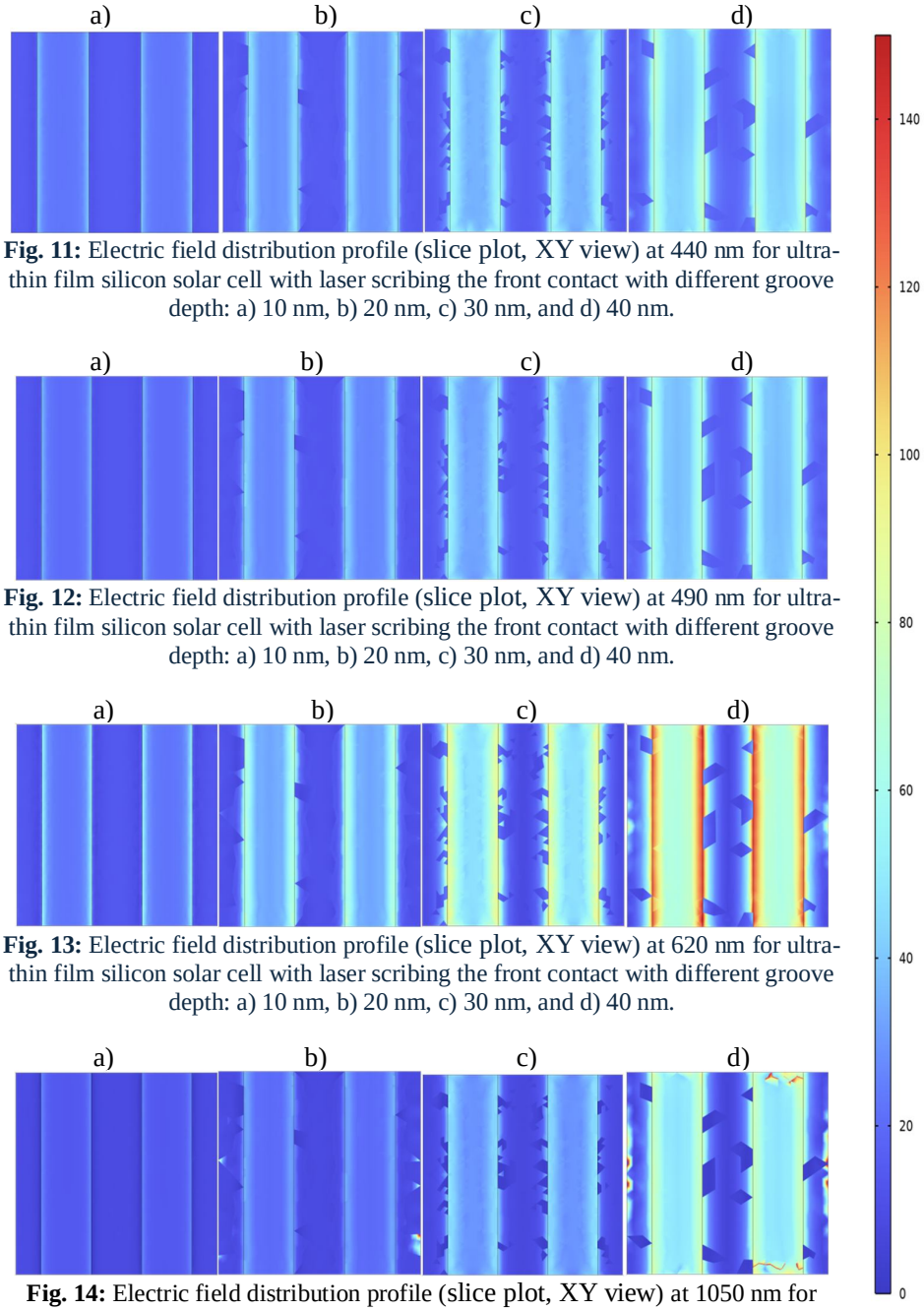

Fig. 11: Electric field distribution profile (slice plot, XY view) at 440 nm for ultra-thin film silicon solar cell with laser scribing the front contact with different groove depth: a) 10 nm, b) 20 nm, c) 30 nm, and d) 40 nm.

Fig. 12: Electric field distribution profile (slice plot, XY view) at 490 nm for ultra-thin film silicon solar cell with laser scribing the front contact with different groove depth: a) 10 nm, b) 20 nm, c) 30 nm, and d) 40 nm.

Fig. 13: Electric field distribution profile (slice plot, XY view) at 620 nm for ultra-thin film silicon solar cell with laser scribing the front contact with different groove depth: a) 10 nm, b) 20 nm, c) 30 nm, and d) 40 nm.

Fig. 14: Electric field distribution profile (slice plot, XY view) at 1050 nm for ultra-thin film silicon solar cell with laser scribing the front contact with different groove depth: a) 10 nm, b) 20 nm, c) 30 nm, and d) 40 nm.

Table 2. Performance comparison of the scribed laser front contact layer silicon solar cell with different groove depths.

Groove depth (nm)	Reference cell	10	20	30	40
Normalized absorption	0.05	0.14	0.17	0.23	0.33
$G_{ph} \times 10^{24}$ ($m^{-3}.s^{-1}$)	0.34	0.74	0.87	1.12	1.5
J_{ph} (mA/cm^2)	4.06	12.92	15.09	19.13	24.66

It was observed that the behavior of the electric field for all resonance wavelengths reflects the absorption of incident light and hence boosting in electric field via the plasmonic effect.

Limitations of the work included small cell dimensions of the proposed cell and manufacturing cost.

4. Conclusion

The extracted results showed clear improvements in ultra-thin-film silicon solar cells using laser scribing for the gold layer. LPRS (near-field) depends mainly on the light absorbed via enlarged gold surface area and light trapping, enhancing absorption through local surface plasmon polariton (near-field) or by scattering (far-field). Performance enhancement of the optical properties was (0.33, 1.5 $m^{-3}.s^{-1}$, 24.66 mA/cm^2) for normalized absorption, photo-generation rate, and photocurrent density, respectively. The increasing of absorption was leading to an increment in the photo-generated rate, reaching to the final result of a rise in the produced photocurrent. The depth of the scribed groove influenced clearly on the cell performance, the deepest groove (40 nm) performs the best, representing the thinnest gold (10 nm remaining), minimizing optical losses and increased absorption at resonance wavelengths. COMSOL is distinguished in handling complex multiphysics simulations, such as electromagnetic waves, multi-layered thin films, and field distributions for absorption efficiency. The proposed cell advances high-efficiency ultra-thin film silicon designs.

References

[1] AL-Hamdani, A., Blawa, B., & Al-Bayati, E. M. (2011). Hybrid (Luminescent and Fresnel) Concentrators to Improve Solar Panel Conversion Efficiency. Baghdad Science Journal, 8(2), 20. https://doi.org/10.21123/bsj.2011.8.2.577-580.
[2] Geng, C., Chen, X., Li, S., Ding, Z., Ma, W., Qiu, J., ... & Fan, H. J. (2021). Graphene quantum dots open up new prospects for interfacial modifying in graphene/silicon Schottky barrier solar cell. Energy Material Advances. DOI: 10.34133/2021/8481915.
[3] Abd alkareem Fadhil, E., & Abdullah, M. M. (2020). CdSe/ZnS core/shell for luminescent solar concentrator. Iraqi Journal of Science, 1645-1649. https://doi.org/10.24996/ijs.2020.61.7.12.
[4] Kong, X., Zhang, L., Liu, B., Gao, H., Zhang, Y., Yan, H., & Song, X. (2019). Graphene/Si Schottky solar cells: a review of recent advances and prospects. RSC advances, 9(2), 863-877. DOI: 10.1039/C8RA08035F.
[5] Sibu, G. A., Gayathri, P., Akila, T., Marnadu, R., & Balasubramani, V. (2024). Manifestation on the choice of a suitable combination of MIS for proficient Schottky diodes for optoelectronic applications: A comprehensive review. Nano Energy, 125, 109534. https://doi.org/10.1016/j.nanoen.2024.109534.
[6] Gatea, M. A., Jawad, H. A., & Hamidi, S. M. (2019). Detecting the thermoplasmonic effect using ellipsometry parameters for self-assembled gold nanoparticles within a polydimethylsiloxane matrix. Applied Physics A, 125(2), 103. https://doi.org/10.1007/s00339-019-2401-7.
[7] Heidarzadeh, H., & Shahabi, T. (2025). Boosting optical current in amorphous silicon solar cells using Multi-layer bimetallic plasmonic Nano-ring structures. Plasmonics, 1-10. https://doi.org/10.1007/s11468-025-02759-1.
[8] Green, M. A. (2009). The path to 25% silicon solar cell efficiency: History of silicon cell evolution. Progress in photovoltaics: research and applications, 17(3), 183-189. https://doi.org/10.1002/pip.892
[9] Heidarzadeh, H., Rostami, A., Matloub, S., Dolatyari, M., & Rostami, G. (2015). Analysis of the light trapping effect on the performance of silicon-based solar cells: absorption enhancement. Applied Optics, 54(12), 3591-3601. doi.org/10.1364/AO.54.003591.
[10] Trompoukis, C., Abdo, I., Cariou, R., Cosme, I., Chen, W., Deparis, O., ... & Depauw, V. (2015). Photonic nanostructures for advanced light trapping in thin crystalline silicon solar cells. physica status solidi (a), 212(1), 140-155. https://doi.org/10.1002/pssa.201431180.
[11] Heidarzadeh, H., Dolatyari, M., Rostami, G., & Rostami, A. (2015, June). Modeling of solar cell efficiency improvement using pyramid grating in single junction silicon solar cell. In 2nd International Congress on Energy Efficiency and Energy Related Materials (ENEFM2014) Proceedings, Oludeniz, Fethiye/Mugla, Turkey, October 16-19, 2014 (pp. 61-67). Cham: Springer International Publishing. https://doi.org/10.1007/978-3-319-16901-9_8

[12] Abdulmalek, N. M., & Jawad, H. A. (2023). Combination of near-field and scattering effects in plasmonic perovskite solar cell including cobalt doped nickel oxide HTL. Optik, 280, 170808. https://doi.org/10.1016/j.ijleo.2023.170808.
[13] de Oliveira, P. R., de Freitas, R. C., de Souza Carvalho, J. H., Camargo, J. R., e Silva, L. R. G., & Janegitz, B. C. (2024). Overcoming disposable sensors pollution: using of circular economy in electrodes application. Current Opinion in Environmental Science & Health, 38, 100540. https://doi.org/10.1016/j.coesh.2024.100540.
[14] Sadhukhan, S., Acharya, S., Panda, T., Mandal, N. C., Bose, S., Nandi, A., ... & Saha, H. (2022). Evolution of high efficiency passivated emitter and rear contact (PERC) solar cells. In Sustainable Developments by Artificial Intelligence and Machine Learning for Renewable Energies (pp. 63-129). Elsevier. https://doi.org/10.1016/B978-0-323-91228-0.00007-0.
[15] Chen, Y., Du, C., Sun, L., Fu, T., Zhang, R., Rong, W., ... & Shi, D. (2021). Improved optical properties of perovskite solar cells by introducing Ag nanopartices and ITO AR layers. Scientific Reports, 11(1), 14550. https://doi.org/10.1038/s41598-021-93914-1.
[16] Mehrpanah, A., Saghai, H. R., Sakkaki, B., & Daghigh, A. (2025). Design of Graphene-Based Core/Shell Nanoparticles to Enhance the Absorption of Thin Film Solar Cells. Plasmonics, 20(6), 3051-3057. https://doi.org/10.1007/s11468-024-02476-1.
[17] Singh, G., & Verma, S. S. (2019). Design and analysis of thin film GaAs solar cells using silver nanoparticle plasmons. Photonics and Nanostructures-Fundamentals and Applications, 37, 100731. https://doi.org/10.1016/j.photonics.2019.100731.
[18] Elshorbagy, M. H., García-Cámara, B., López-Fraguas, E., & Vergaz, R. (2019). Efficient light management in a monolithic tandem perovskite/silicon solar cell by using a hybrid metasurface. Nanomaterials, 9(5), 791. https://doi.org/10.3390/nano9050791.

التاثير البلازموني على اداء الخلية الشمسية السليكونية فائقة الدقة ذات طبقة الذهب الامامية المحفورة بالليزر

رسل احمد ذهب*، حسين علي جواد

فرع التطبيقات الهندسية والصناعية، معهد الليزر للدراسات العليا، جامعة بغداد، بغداد، العراق

البريد الالكتروني للباحث: *rusul.ahmed2301m@ilps.uobaghdad.edu.iq*

الخلاصة: الحفر بالليزر لطبقة المعدن الأمامية من الخلية السليكونية فائقة الدقة تعتبر احد الطرق التي تحسن الأداء من خلال زيادة المساحة السطحية لطبقة المعدن والتي تؤدي إلى امتصاص اعلى. لهذا الغرض، تم تصميم خلية سليكونية فائقة الدقة ذات الطبقة الأمامية من الذهب بالأبعاد nm^3 (400×400×900) للطول والعرض والارتفاع تواليا حيث كان سمك طبقة الذهب هو 50 nm. تم اجراء عملية الحفر على طبقة الذهب بمختلف الأعماق (10, 20, 30, 40) nm وبعرض ثابت قدره 100 nm. استخدم البرنامج الحاسوبي COMSOL بطريقة العناصر المحدودة FEM لتصميم وبحث النتائج رقميا. أظهرت النتائج المستخلصة ان التيار الصوئي النتاتج من الخلية المفترضة هو $26.66\ mA/cm^2$ والذي يمثل اعلى قيمة تيار عند العمق 40 nm . يمكن ان نستنتج بان الخلية السليكونية ذات دقة الذهب المحفورة تؤدي إلى زيادة التيار المنتج في الخلية مما يؤدي إلى تحسن الأداء.